



PAPER • OPEN ACCESS

## Soft shadow images

To cite this article: Johannes Grebe-Ellis and Thomas Quick 2023 *Eur. J. Phys.* **44** 045301

View the [article online](#) for updates and enhancements.

### You may also like

- [Transition temperature and the equation of state from lattice QCD. Wuppertal-Budapest results](#)  
Szabolcs Borsanyi, Gergely Endrodi, Zoltan Fodor et al.
- [Application of rule-based data mining techniques to real time ATLAS Grid job monitoring data](#)  
R Ahrens, T Harenberg, S Kalinin et al.
- [Energy-Variation Analysis and Orbit-Complexity Quantification](#)  
Fotios Kasolis and Markus Clemens

# Soft shadow images

Johannes Grebe-Ellis\*  and Thomas Quick 

University of Wuppertal, Faculty of Mathematics and Natural Sciences, Gaußstraße 20,  
D-42119 Wuppertal, Germany

E-mail: [grebe-ellis@uni-wuppertal.de](mailto:grebe-ellis@uni-wuppertal.de) and [quick@uni-wuppertal.de](mailto:quick@uni-wuppertal.de)

Received 2 November 2022, revised 1 March 2023

Accepted for publication 27 March 2023

Published 11 May 2023



CrossMark

## Abstract

In traditional optics education, shadows are often regarded as a mere triviality, namely as silhouettes of obstacles to the propagation of light. However, by examining a series of shadow phenomena from an embedded perspective, we challenge this view and demonstrate how in general both the shape of the object and light source have significant impact on the resulting soft shadow images. Through experimental and mathematical analysis of the imaging properties of inverse objects, we develop a generalized concept of shadow images as complementary phenomena. Shadow images are instructive examples of optical convolution and provide an opportunity to learn about the power of embedded perspective for the study of optical phenomena in the classroom. Additionally, we introduce the less-known phenomenon of the bright shadow.

Keywords: soft shadow image, bright shadow, embedded perspective, convolution, complementarity

(Some figures may appear in colour only in the online journal)

## 1. Introduction

In optics teaching it is common to view shadows as trivial phenomena, simply as silhouettes of opaque obstacles which prevent the propagation of light [1]. However, a simple experiment can cause confusion (figure 1, upper row): a small round cardboard disc is positioned in front of an annular light source so that its shadow falls on a projection screen. Moving the disc

\* Author to whom correspondence should be addressed.



Original content from this work may be used under the terms of the [Creative Commons Attribution 4.0 licence](https://creativecommons.org/licenses/by/4.0/). Any further distribution of this work must maintain attribution to the author(s) and the title of the work, journal citation and DOI.

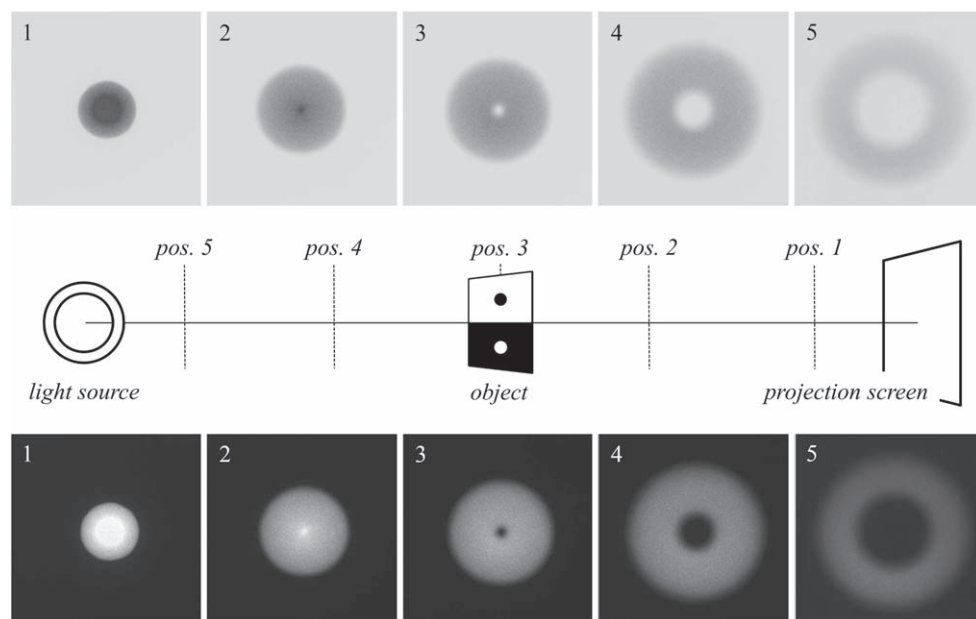


**Figure 1.** Inverse objects: a small round cardboard and a panel opening with the same size ( $\varnothing = 5$  cm) are illuminated with an annular light source ( $\varnothing = 25$  cm, middle). The photographs in the upper and the bottom row show the transformation of the shadow images on the projection screen, while the inverse objects are moving towards the light source.

from the screen towards the source, we observe a remarkable change in the shadow image. The shadow of the disk takes the form of a *ring*—a challenge to the conventional concept of shadow formation [2], which raises the question: how the shadow of the cardboard disk and the dark image of the annular light source are related? A similar, more familiar situation can be found in pinhole imaging. When the obstacle is replaced by a geometrically equivalent aperture (i.e. swap the transmissive and occluding region), the geometrical imaging properties remain unchanged. We get a bright ring on the screen: the pinhole image of the light source (figure 1, bottom row). The dark image, sometimes called the *anti-pinhole* or *pinspeck image* [3, 4] and the bright pinhole image of the light source are complementary phenomena.

There is a long-standing tradition in teaching optics to study special cases of shadow formation where either the extent of the light source or the extent of the aperture is neglected. Hard shadows as produced by point-like light sources are easy to model because they represent projections of the illuminated objects. On the other hand, the pinhole camera is about producing bright images of the light source. In both cases, the geometric influence of the imaging element is suppressed. As special cases, however, they are only poles of a wide range of possible imaging geometries (figures 1 and 2), which generally both image and are imaged, and further produce intriguingly appealing shadow images. One aim of this paper is to expand and generalize the concept of shadow to include this variety of shadow phenomena for the context of optics lessons.

In computer graphics technology, the question of how to render realistic soft shadows for complex lighting scenes has sparked vast research efforts which led to an advanced understanding of shadow formation on the base of what we call the *embedded perspective* [5–7]. Shadow is defined here as it is experienced standing in the shadow oneself: as an *occlusion*

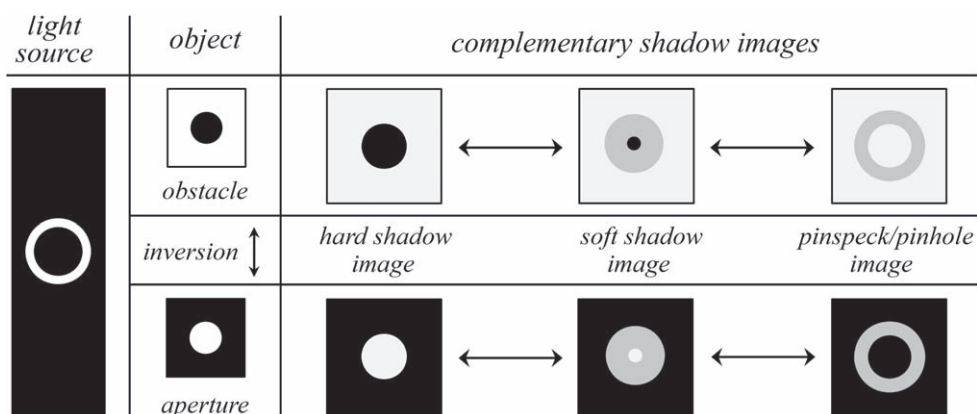


**Figure 2.** For terminology: an object can be either an *aperture* or an *obstacle*, always referring to the totality of the transmissive and occluding region. Hard shadows are projections of the objects. The pinhole or pinspeck image is an image of the light source. Soft shadows are always mixtures of the geometry of object and light source.

*phenomenon*. The approach can provide a useful explanation that makes complex irradiance distributions more accessible. For example, the puzzle of the dark ring from the beginning can be quickly solved by looking at the spatial layout of light source and obstacle from the location of the shadow: viewed from the illuminated center of the dark ring, the annular light source is fully visible.—Although the approach of the embedded view is reasonable and powerful, it has been uncommon in optics education so far. Thus another aim of this paper is to demonstrate the explanatory power of the embedded perspective as a possible approach to shadow imaging in optics teaching.

The paper is organized as follows: in section 2 we present shadow phenomena from nature, everyday life, and the laboratory, which exemplify various cases of the totality shown schematically in figure 2. They provide the starting point for an exploration of the relevant conditions in section 3. On the basis of the embedded perspective we describe the irradiance distribution in the shadow image and show that this corresponds to a convolution of light source and object [8]. We investigate the transformation properties of shadow images and we show the invariance of the imaging conditions under inversion of the object [9]. We arrive at the little-known fact that shadows are complementary phenomena. In this context, we describe another complementary shadow phenomenon that has not yet received proper attention. The *bright shadow* occurs by inverting the light source [10]. In section 4 we give a simple mathematical model for the irradiance distribution within shadow images which can reproduce all the phenomena described in this paper.

## 2. Shadows in the laboratory, nature and everyday life

To say that the edges of shadows appear smooth because the light source is extended, is not wrong, but it downplays the fact that there is a characteristic imprint of the source geometry that can be discovered in the shadow image. Figure 3 shows shadow images of pliers illuminated with various shapes of light sources. The distances between light source, pliers and screen remain unchanged, only the geometry of the light source is varied (shown at the bottom left of each picture). The shadow image obviously refers not only to the pliers as an obstacle, but also to the particular shape of the light source, which gives it a characteristic,

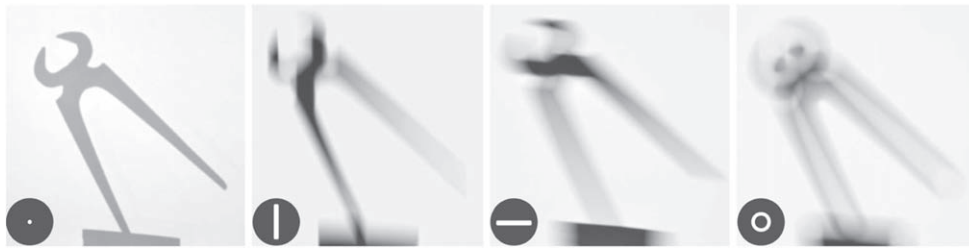


**Figure 3.** Shadow images of pliers illuminated with different light source geometries.

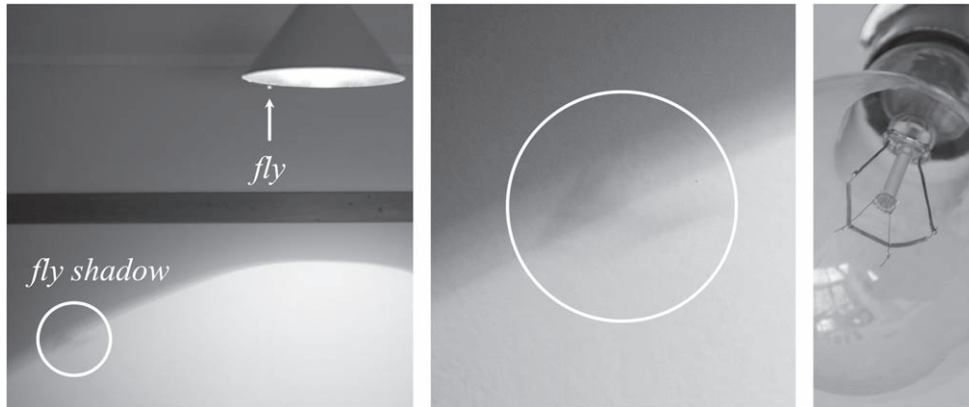


**Figure 4.** Shadow of a fly during its journey on a lampshade. That it is the fly's shadow, can only be recognized by the movement. It has no resemblance to the fly but shows the dark image of the illuminating filament.

aesthetic appearance. It seems as if the sharp outline of the pliers' shadow has been softened by the shape and orientation of the light source—the shadow image could be thought to have been created by drawing with a pen whose tip has the shape of the light source geometry [9, 11].

While in figure 3 the geometry of the light source mainly influences the penumbra of the pliers' shadow, the next example from everyday life shows that the shadow image can adopt the source geometry completely [12]. In figure 4, a fly wanders along the edge of a lampshade and creates a shadow on the wall. The shadow image takes on the very different but distinct shape of a filament, which is a dark image of the incandescent filament of the bulb. Similar transformations of shadow images can be discovered in everyday life [13, 14]. Figure 5 shows a bouncing ping-pong ball illuminated from above by a rod light. Whenever the ball's distance from the ground increases, its shadow stretches in a direction determined by the orientation of the rod light: the shadow becomes the dark image of the latter.

Though somewhat more subtle, the influence of source geometry is often noticeable at shadow edges. For example, where the trunk of a tree or a street light meets the ground the shadows always appear much sharper, richer in contrast and darker than the shadow areas from higher up. As the distance from the obstacle increases, the shadows become softer and lighter, i.e. the geometry of the circular sun makes a stronger influence. When we look at our own shadow in sunlight, the penumbra always carries inscribed images of the Sun, since the Sun has an extension of about 0.5 degrees (figure 6).

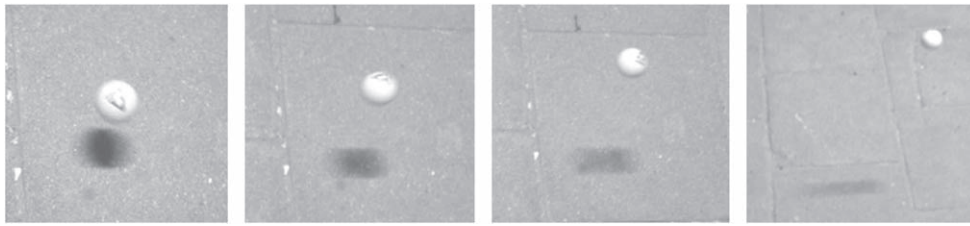


**Figure 5.** Shadow of a bouncing ping-pong-ball illuminated by a rod light.



**Figure 6.** Shadow image of crossed fingers on a sunlit wall. The larger the distance to the wall, the more dominant the image of the solar disk: ‘sun coins’. Fotos: Laila Ellis

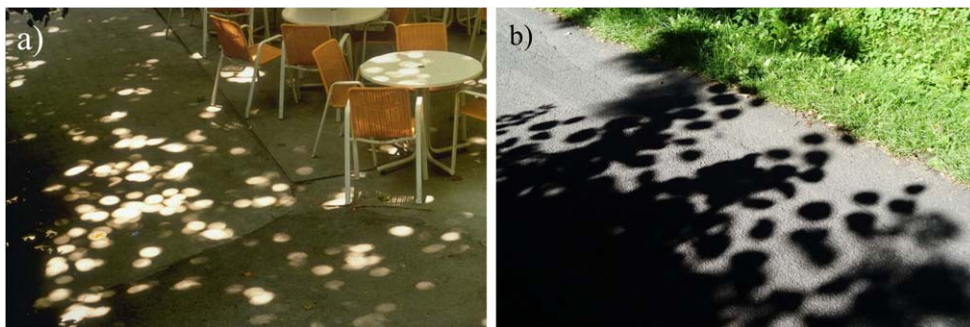


**Figure 7.** The leaves of a tree creates both pinhole images (a) and pinspeck images (b) of the Sun (reprinted with kind permission of H-J Schlichting).

More familiar than imaging with obstacles is imaging with apertures [15–17]. Figures 6 and 7 show ‘sun coins’ (in German called ‘Sonnentaler’), i.e. pinhole images of the Sun on the ground (figure 7(a)) under the high canopy of a tree, which are described frequently in the literature [18–20]. They are the complementary counterpart to the dark ‘sun coins’ [21] in figure 7(b), where the imaging elements are the leaves themselves. The extent to which the appearance of shadows in nature is influenced by the size and shape of the solar disk is particularly evident in the transformations of shadow images during the covering phases of a solar eclipse (figure 8). The symmetry of the light sources in the previous examples hid the fact that the pinhole image is point-symmetrically mirrored. Figure 9 shows the transition of complementary shadow images for an L-shaped geometry of the light source.



**Figure 8.** Images of the partially eclipsed sun during a solar eclipse. Foto: Bill Gozansky.

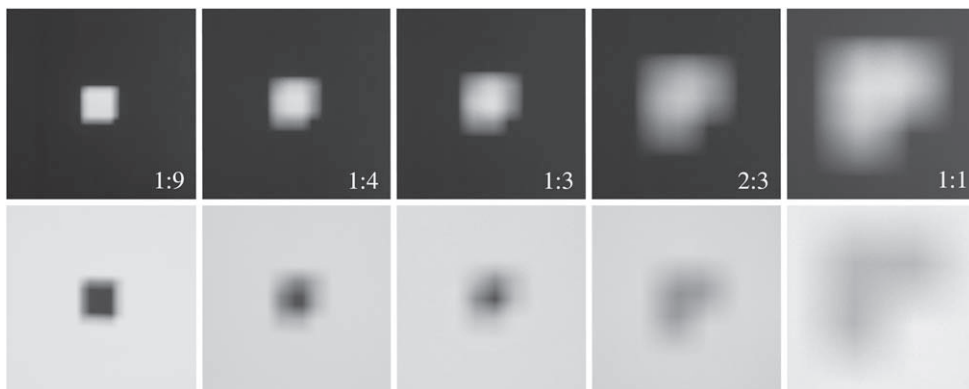


**Figure 9.** Complementary shadow images created with an L-shaped light source ( $9 \times 9$  cm) and a square geometry of the object ( $2.25 \times 2.25$  cm) (setup shown in figure 13). The distance between the light source and the projection screen was 2.4 m. The ratio of the distances to the object is given in the upper row.

Little-known so far is the *bright shadow* [10]. It appears, for example, in the interplay of two obstacles standing offset to each other, which are illuminated by an extended light source. It can be discovered easily in the diffuse shadow of a bar placed on a table in front of a window in the glare of the bright sky if you move a second bar in between. Then a bright and relatively sharp stripe appears in the diffuse shadow of the first bar (figure 10). Its trace on the table refers to the position of the moving bar, which so to speak acts as an ‘inverse light source’. Similarly, the vertical bars of a window front become visible as bright stripes in the diffuse shadow of an upright note-taking pencil. Figure 11 shows what matters for the formation of bright shadows. If an extended light source (here a rod lamp) is darkened at a

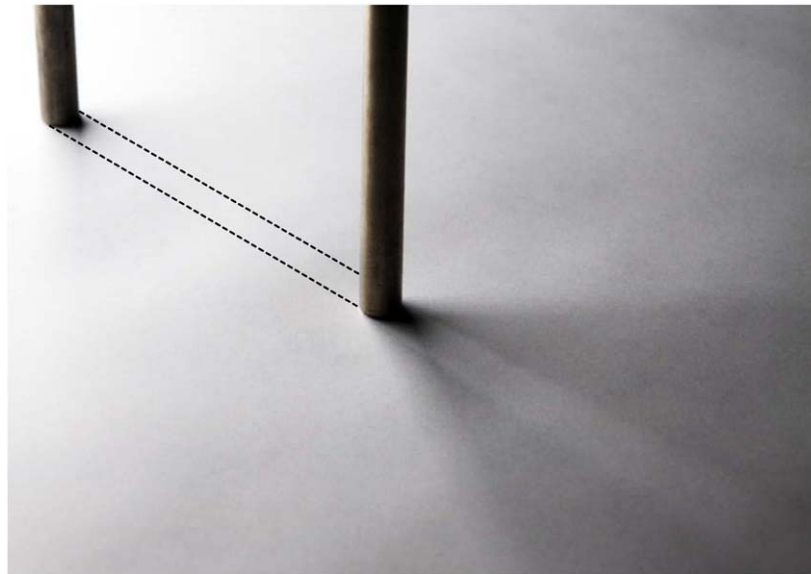


**Figure 10.** The ordinary shadow of a bar in diffuse lighting from a window to the bright sky (top left) is maximally blurred. Where the darkening by a second bar is not effective because of the occlusion by the first, it is brighter than in the surrounding area.



**Figure 11.** A square frame of paper, suspended by a nylon thread, is illuminated by a horizontal rod lamp (a). If the lamp is covered at one point, a bright shadow appears in the diffuse shadow of the frame (b and c).

certain place (figure 11), a relatively sharply contoured but now bright shadow image of the object appears in the diffuse shadow of the object.

The showcases mentioned exemplify how diverse and impressively beautiful the world of shadow images is. What can we learn from these examples? In general, both the shape of the light source and the shape of the object interact in shadow images. They are involved both as imaging and as being imaged. Seemingly complicated shadows are often created by the intertwining of unusual geometries of light sources and object. At first glance, which of the effective geometries predominates in the shadow image depends on the relative distances between the light source, object and projection screen. Closer examination in the next section shows that what matters is the relative size of the light source and the object—as seen from the projection screen.



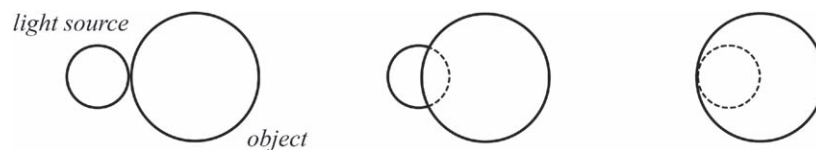


**Figure 12.** View from the embedded perspective on light source and object while moving from the left into the shadow. At the border of penumbra, the light source is just unobscured (left). In the penumbra, the light source is partially obscured: the smaller the unobscured part, the darker the penumbra (center). At the boundary from penumbra to umbra, the light source is just fully obscured (right).

### 3. Exploring soft shadow images

#### 3.1. Investigating shadow images from the embedded perspective

As it is known from the observation of solar eclipses, the formation of shadows can be explained by relating the irradiance of a given point in the shadow to the degree of occlusion of the light source by the object—as seen from that point on the projection screen (where it can be a human eye or a technical eye, e.g. a detector) [22]. In contrast to the detached perspective typically discussed in the side view, here the eye is part of the setup. We therefore refer to this view from the screen as *embedded perspective*. It is always used when considering what a detector ‘sees’, i.e. when thinking through the conditions of an optical imaging system not only from the light source but also in the opposite direction, i.e. from the detector.

In the case of shadow images, these conditions are given by very simple perspective and parallax properties of the spatial interplay between light source and object with respect to the projection screen (figure 12): no shadow is where the light source is unobscured from; penumbra is where only part of the light source can be seen from; umbra is where the light source is fully obscured from. To illustrate the approach with an experiment we drilled a small hole in the projection screen of the setup shown in figure 13. It projects a pinhole image of the lighting situation onto a second semitransparent screen. The pinhole image then shows what is visible from the respective pinhole position while moving the first screen through the shadow image (figure 14, 1–6 on the right): a projection of the object into the plane of the light source.

In optics education, however, the embedded perspective has been rather uncommon, although it has didactic potential. It links the respective optical conditions to the student’s own experiences, thereby encouraging a more phenomenon-based understanding of optical concepts. In the German literature there is a phenomenological tradition in optics teaching where the change between embedded and detached perspective as a powerful exploration tool has long been established [10, 23, 24]. The idea of teaching optics close to the phenomena (‘the world through my eyes’), especially in the early grades, has been increasingly taken up in recent years and investigated in empirical studies of phenomenological optics teaching [25–29].

#### 3.2. Adjusting the conditions of shadow images

How bright it is at a given point on the screen depends on the degree of occlusion of the *apparent sizes* of light source and object in the field of view of the embedded observer. As known from astronomy the apparent size can be quantified using the concept of solid angle,

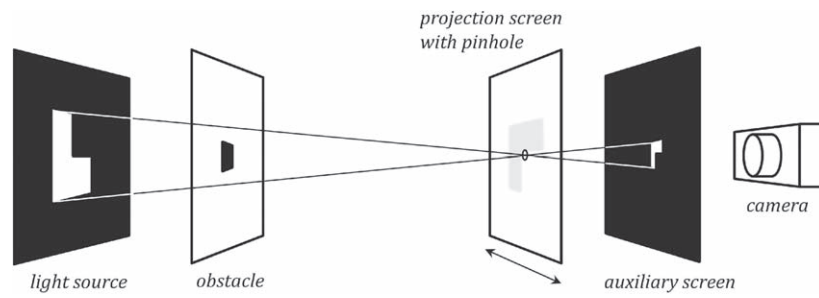


**Figure 13.** Experiment to illustrate the embedded perspective. While the projection screen with the pinhole is moved through the shadow image, the respective pinhole image shows what can be seen from the location of the pinhole: a projection of the object (here an obstacle) into the plane of the light source (figure 14, right).

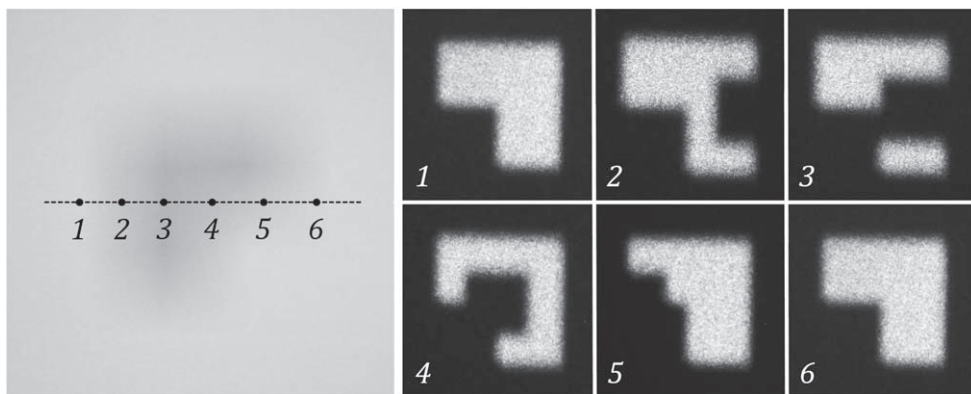


**Figure 14.** Left: Photo of a shadow image at the projection screen from the setup shown in figure 13 with six pinhole positions. Right: the corresponding pinhole images show the transformation of the occlusion situation as seen from the respective pinhole position in the shadow image: while the ‘pinhole eye’ moves from position 1 to 6, the square obstacle passes in front of the light source due to parallax from right to left.

which is measured with respect to the observer’s eye. In the case of an obstacle, the solid angle describes the opaque part of the object, while in the case of an aperture, it describes the transmissive part of the object. In the following, we will focus on the case of an obstacle and later return to the general case of objects, which includes the inverse case of the aperture (subsection 3.5).

We assume that the shadow images under consideration are created in the vicinity around the optical axis. Then we can simplify the solid angles of light source  $\Omega_l$  and obstacle  $\Omega_o$  to appear approximately constant for the observer. That means for different positions  $P$  on the screen the seen sizes of light source and obstacle only shift to each other due to parallax without perspective foreshortening. Then we can approximate  $\Omega_l \approx A_l / (d_1 + d_2)^2$  and  $\Omega_o \approx A_o / d_1^2$  for the solid angles of the light source and the obstacle, where  $A_l$  and  $A_o$  are the absolute areas of the light source and obstacle,  $d_1 + d_2$  is the distance from the light source to the screen and  $d_1$  is the distance from the obstacle to the screen. For small angles  $\varepsilon_1$ ,  $\bar{\Omega}_l \approx \bar{A}_l / (d_1 + d_2)^2$  should then be the solid angle of the seen, i.e. unoccluded, area of the light source for a certain occlusion of the light source by the obstacle.

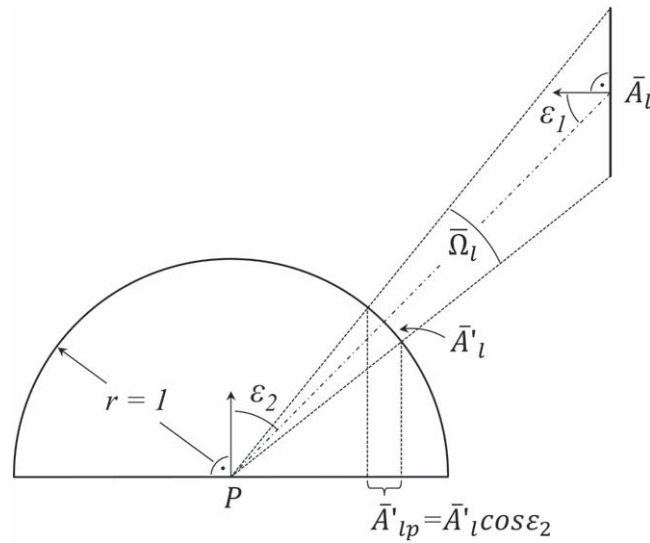


**Figure 15.** To the observer in  $P$ , the light source  $\bar{A}_l$  appears at solid angle  $\bar{\Omega}_l$ , whose projection  $\bar{\Omega}_{lp} = \bar{\Omega}_l \cos \varepsilon_2$  is a measure of the irradiance in  $P$ . For small angles  $\varepsilon_2$ ,  $\bar{\Omega}_{lp} \approx \bar{\Omega}_l$ .

On the other hand, the irradiance on a given surface is also affected by its orientation  $\varepsilon_2$  relative to the light source, which is determined by the projected solid angle  $\bar{\Omega}_{lp}$  (figure 15). This is especially apparent in the case of Sun position-dependent illumination, where the amount of light received by a surface is influenced by the position of the Sun in the sky. Although the seen solid angle of the Sun remains approximately constant, the setting Sun near the horizon delivers much less light than a Sun in the zenith. For small angles  $\varepsilon_2$  the projected solid angle can be approximated by the solid angle itself, i.e.  $\bar{\Omega}_{lp} \approx \bar{\Omega}_l$ . Thus, the solid angle can be equated to the unoccluded portion of the light source that is visible to the observer.

If we further assume that the light source is Lambertian with constant radiance, then the irradiance  $E(P)$  at a given point  $P$  on the screen is approximately proportional to the solid angle  $\bar{\Omega}_l$  for a certain occlusion of the light source by the obstacle. It holds that  $E(P) \propto \bar{\Omega}_l$  (more in section 4).

Although the idea of the embedded perspective applies much more generally, shadow images can be easily modeled under these assumptions and it is approximately satisfied in most teaching experiments.

### 3.3. The shadow image as convolution

To determine the solid angle  $\bar{\Omega}_l$  of the unobscured light source, one must appropriately weight the solid angle  $\Omega_l$  of the complete area light source with the solid angle  $\Omega_o$  of the obstacle for each location  $P$  on the screen. Mathematically, this process corresponds to a convolution operation between the geometries of the light source and obstacle, thus shadow imaging is a beautiful example of convolution [8, 30].

Qualitatively speaking, we represent the light source and obstacle as functions in the source plane. We therefore project the obstacle into the plane of the light source so that  $\Omega_o = A_o/d_1^2 = A_o'/(d_1 + d_2)^2$  applies, with  $A_o'$  the projection of the obstacle's area  $A_o$  into the source plane. For simplicity, we consider the one-dimensional case here; the general case

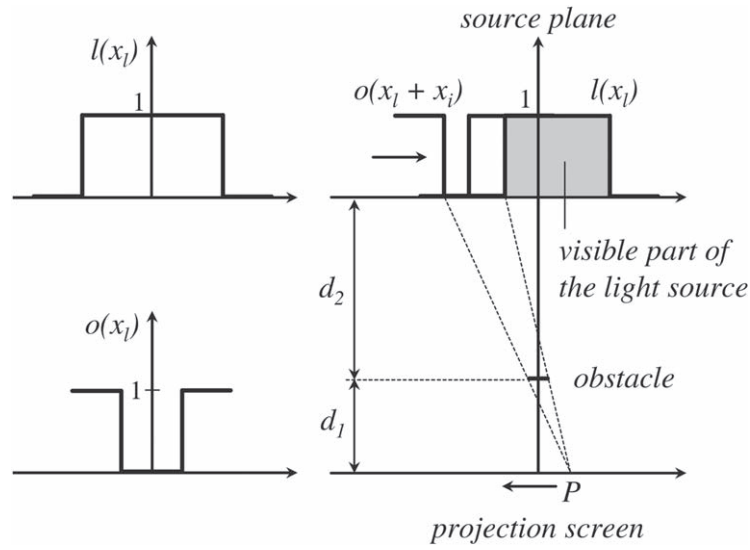


**Figure 16.** To illustrate the convolution of light source and projected obstacle they are expressed as functions in the source plane. Right: if the observer  $P$  moves on the projection screen, the obstacle shifts in the opposite direction in the source plane. The visible part of the source then corresponds to the overlap of the two functions of source and obstacle.

will be examined in more detail in section 4. Let  $l(x_l)$  and  $o(x_l)$  be representative functions of the light source and the projected obstacle in the source plane as shown in figure 16. The integration  $\int l(x_l) dx_l$  and  $|\int o(x_l) dx_l|$  respectively give the ‘areas’ of the light source  $A_l$  and the projected obstacle  $A_o'$ . If the observer moves to the left on the screen, the obstacle moves to the right in his field of view, i.e. the projected obstacle shifts with some  $x_i$ , so  $o(x_l + x_i)$ . The ‘area’ of the unoccluded light source  $A_l$  is then given by  $\int l(x_l) o(x_l + x_i) dx_l$  [31]. Because of  $E(P) \propto \bar{\Omega}_l$  for the irradiance  $E(x_i)$ , the following applies

$$E(x_i) \propto \int_{-\infty}^{\infty} l(x_l) o(x_l + x_i) dx_l.$$

With the substitution  $x_l = -x_l'$  we get the definition of the convolution product

$$E(x_i) \propto \int_{-\infty}^{\infty} l(-x_l') o(x_l - x_l') dx_l' = l(-x_i) * o(x_i).$$

### 3.4. Transformation conditions of soft shadow images

So far, we related the transformation of soft shadow images to the change in the relative distances of the light source, obstacle, and projection screen (figure 1): as the obstacle moves closer to the screen, the shadow image almost assumes its shape. In the other limiting case the obstacle moves toward the source and the pattern converges with the shape of the source. Evidently not every arbitrary obstacle produces the image of the light source when approaching it. And with respect to the Sun, an indication of the change of distance is meaningless. The relevant conditions are easily understood from the embedded perspective: the darkness of the shadow is determined by the ratio of the solid angles of the obstacle  $\Omega_o$

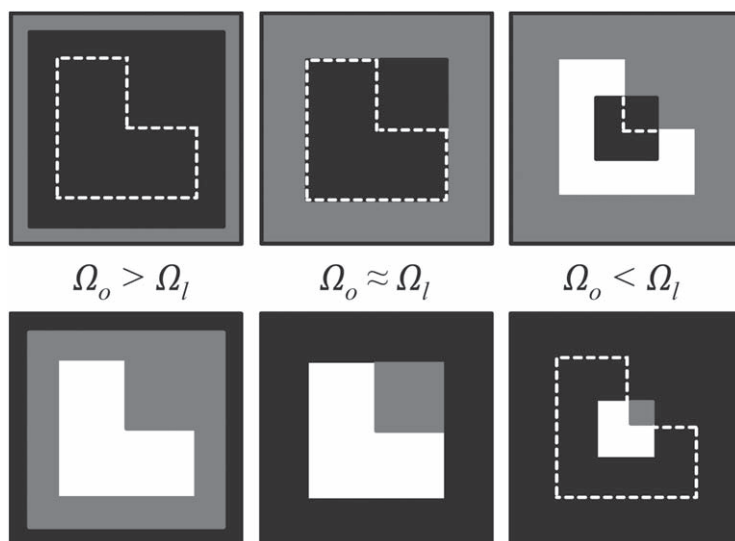


**Figure 17.** Shadow images are determined by the ratio of the solid angle  $\Omega_l$  of light source (L-shape, white) and object  $\Omega_o$  (square obstacle above, corresponding aperture below, both black; background: grey) for cases (i)–(iii), seen from the embedded perspective. The case  $\Omega_o < \Omega_l$  in the top row on the right corresponds to the pinhole image no. 4 in figure 14.

and the light source  $\Omega_l$ , as seen from the screen. As long as the distance between the light source and the projection screen remains unchanged,  $\Omega_l$  is constant. For the ratio to  $\Omega_o$ , this leads to the following characteristic cases: if  $\Omega_o > \Omega_l$  holds, the light source is fully occluded for an extended area at the screen. The shadow image is dominated by the umbra and thus by the geometry of the obstacle. In the reverse case  $\Omega_o < \Omega_l$ , i.e. the seen size of the obstacle is smaller than the light source. The obstacle can only cover a small part of the light source. It thus changes from being the *imaged* element to being the *imaging* element. The shadow image is dominated by the penumbra and thus by the geometry of the light source. In between is a position where the magnitude of  $\Omega_o$  and  $\Omega_l$  are in the same range:  $\Omega_o \approx \Omega_l$ . The visible size decreases with the square of its distance from the embedded observer. Thus the image shows a balance between the two shapes when  $A_o/A_l = d_1^2/(d_1 + d_2)^2$ . In summary, referring back to the scheme in figure 2, the following three cases can be distinguished (figure 17, top row) [9]:

- (i)  $\Omega_o > \Omega_l$ : if  $\Omega_o$  is larger than  $\Omega_l$ , the image of  $A_o$  predominates  $\rightarrow$  *hard shadow*
- (ii)  $\Omega_o \approx \Omega_l$ : the image shows a balanced mixture of shapes  $A_o$  and  $A_l \rightarrow$  *soft shadow*
- (iii)  $\Omega_o < \Omega_l$ : if  $\Omega_o$  is smaller than  $\Omega_l$ , the image of  $A_l$  predominates  $\rightarrow$  *pinspeck image*

If the light source is very small ( $\Omega_o \gg \Omega_l$ ) we obtain very sharply contoured shadow images of the obstacle, which belong to the common notion of shadows.

### 3.5. Complementarity of shadow images

Principles of complementarity are introduced in optics mainly to order color spaces, i.e. to define the complement of a given color [32]. Somewhat generally, the complement is understood to be something like the completing counterpart of a whole, where the whole

remains invariant under certain conditions. Following on from this, we call two irradiances  $E_1$  and  $E_2$  complementary to each other if they satisfy the relation

$$E_1(P) + E_2(P) = E_0. \quad (1)$$

For a given irradiance  $E_0$  (the ‘whole’), the irradiance  $E_2 = E_1^C$  is then complementary to  $E_1$ , where the ‘C’ stands for ‘complementary’ [33, 34]. As we will now see, inverting the object (obstacle  $\rightleftharpoons$  aperture) of a given irradiance distribution produces a second one for which this criterion is satisfied *for all* locations on the screen.

To verify the complementarity relation for shadow imaging we consider the following. Inverting the object means swapping the opaque and the transmissive parts of the object while keeping the geometrical properties invariant (figure 17 top row and bottom row). From the embedded perspective, however, this also means that the visible and non-visible parts of the light source are swapped. If  $\Omega_l$  is the total solid angle of the light source, and  $\bar{\Omega}_l$  the unoccluded, i.e. visible part of the source for a given position  $P$  on the screen then we get  $\bar{\Omega}_l^C = \Omega_l - \bar{\Omega}_l$  as the visible part of the source in the inverted case. The previously invisible parts of the source are now visible. As discussed the irradiance  $E(P)$  is under the specified simplifications proportional to the magnitudes of the respective solid angles of the visible part of the area light source, i.e.  $E_1(P) \propto \bar{\Omega}_l$ ,  $E_2(P) \propto \bar{\Omega}_l^C$  and  $E_0 \propto \Omega_l$ , where  $E_0$  is the constant irradiance at  $P$  due to the unoccluded light source with the fixed solid angle  $\Omega_l$ . Because this holds for every point on the screen, it results in  $E_2(P) = E_0 - E_1(P)$  and the complementarity relation (1) is fulfilled. Therefore  $E_2 = E_1^C$ . In this sense, all pairs of images in the top and the bottom row from figure 1 respectively figure 9 are complementary to each other.

The above mentioned transformations (i–iii) are invariant under inversion of the object, i.e. if we replace an obstacle by a geometrically equivalent aperture, where  $\Omega_o$  now describes the solid angle of the transmissive part of the aperture (see figure 17). The first case (i) with  $\Omega_o > \Omega_l$  leads to the image of the aperture where the geometry of the source approximately being suppressed. The third case (iii) with  $\Omega_o < \Omega_l$  leads to the pinhole image where the solid angle of the aperture is small in comparison to the solid angle of the area light source.

### 3.6. Conditions of the bright shadow

Inversion was previously limited to the plane of the object. What happens when the light source is inverted? The interchange of luminous and nonluminous regions in the plane of the light source yields an inversion of the ordinary shadow, called *bright shadow* (figures 10 and figure 11) [10]. An inversion of the radiance can of course only be realized approximately, e.g. by covering an extended luminous field of homogeneous radiance in a limited area. The covered area in the bright environment then corresponds to the ‘inverse light source’.

Initially, we aim to elucidate how the occurrence of brightening in shadows can be comprehended from the embedded perspective. In the setup of figure 10 we used a large window to the bright sky which was partially covered by a bar. Since the important thing here is to cover an area within an extended field of homogeneous radiance, for simplicity we consider the following a ‘one-dimensional’ extended rod light. Figure 18 schematically shows how an upright cylinder  $G_1$  is illuminated with a horizontally aligned, stretched rod light. The inverse light source is realized by the covering part of cylinder  $G_2$ . As in the ordinary case the geometry of  $G_2$  determines the size of the penumbra, the one of  $G_1$  the size of the umbra. The view from the embedded perspective (figure 18, below) makes immediately clear what matters: because the unobscured part of the rod light seen from  $P_2$  is larger than from  $P_1$  and  $P_3$ , it is also the brightest there.

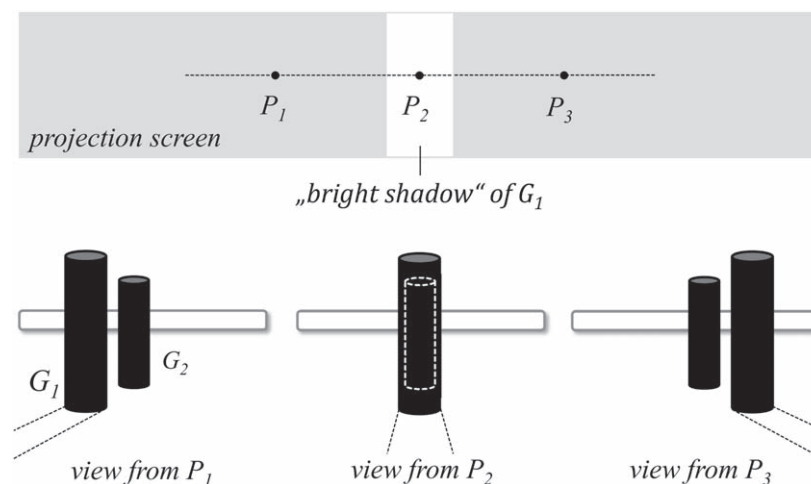


**Figure 18.** Schematic of the bright shadow (top) and the conditional occlusion as seen from the embedded perspective of the projection screen (bottom). By inserting  $G_2$ , it becomes darker everywhere on the projection screen except for the area from where  $G_2$  is masked by  $G_1$  (view from  $P_2$ ). Therefore the bright shadow appears not because this region becomes brighter, but because the surrounding region becomes darker.

To clarify the bright shadows relation to the obstacle, we utilize the transformation conditions outlined in subsection 3.4. We define  $\Omega_o$  again as the solid angle of the obstructing region of the obstacle, and  $\Omega_l$  as the solid angle of the ‘inverse light source,’ which arises from the obstructed area in the extended illuminated field. In figure 11, for example, the condition  $\Omega_o > \Omega_l$  is met. When  $\Omega_o$  is larger than  $\Omega_l$ , the image of  $A_o$  becomes dominant, resulting in a hard but bright shadow.

One might think the bright shadow is a mere trick. In fact, it is nothing more and nothing less than the inverse of the ordinary shadow. The latter arises where the brightening of the dark space by a light source does not become effective because of an obstacle. The bright shadow arises where the darkening of the illuminated space by an inverse light source does not become effective because of an obstacle.

Although the conditions may seem somewhat artificial at first glance, it is easy to discover the bright shadow in nature and in everyday life, you just have to learn to see it [10, 35]. As a more detailed analysis of the inversions presented here shows, these are only partial inversions. A generalization of the issue is beyond the scope of the present article. As has been shown by Rang, a strict generalized complementarity condition requires the inversion of the entire space, i.e. the swapping of the flux density at each point in space, and thus leads to the theory of *bright space* [36].

## 4. Modeling soft shadow images

### 4.1. Assumptions of the model

In the following, we present a simple model for the computation of soft shadow images, which is still elaborate enough to capture all phenomena discussed in this paper (see also [8, 37]). The model is based on the following assumptions:

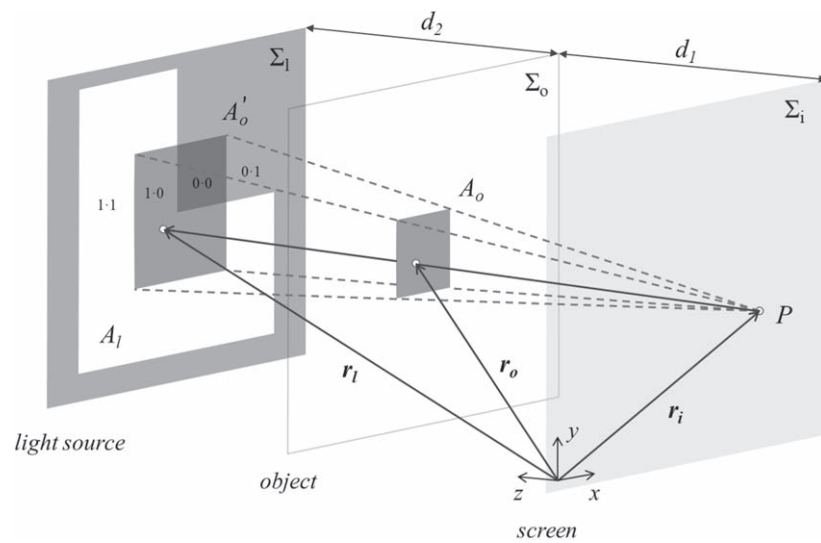


**Figure 19.** Simple geometric model for the generation of shadow images.

- (i) Object and light source are treated as shapes that lie in planes parallel to the screen.
- (ii) The area light source is treated as a Lambertian emitter, i.e. the radiance  $L$  [ $\text{W m}^{-2}\text{sr}^{-1}$ ] is constant over the whole surface and in all directions. For a uniform diffuse emitter, the radiance is given by the radiosity (radiant exitance)  $M$  [ $\text{W m}^{-2}$ ] radiated over the hemisphere, i.e.  $L = M/\pi = \text{const.}$  for all points on the source [38].
- (iii) The shadow image is generated in close proximity to the optical axis on the screen, thereby satisfying the paraxial approximation. As a consequence, we assume that the projected solid angle of  $\bar{\Omega}_l$ , which corresponds to the visible and unobscured light source, remains constant and can be approximated to the solid angle itself. Moreover, we ignore the effect of perspective shortening on the area of the light source and object when they are viewed at oblique angles.
- (iv) The screen is a Lambertian surface, which is a perfect diffusing reflector that exhibits uniform radiance in all directions, and the incoming irradiance is proportional to the radiosity of the surface. Consequently, the shadow image that is observed on the screen can be characterized by the irradiance distribution.
- (v) The object is large with respect to the wavelength of light, which is why effects due to the wave nature of light (e.g. diffraction or interference) are neglected [39]. Physiological and psychological effects, for example, the Machband effect or Koffka's effect are also neglected [40, 41].

#### 4.2. Visible part of the light source

We define a cartesian coordinate system in which the  $xy$ -plane is the plane of the screen and the  $z$ -axis is in the direction of the illuminating source with area  $A_l$  and the object with area  $A_o$  of the occluding part. Parallel to the imaging plane  $\Sigma_i$  (the screen) the object plane  $\Sigma_o$  is positioned at the distance  $d_1$ . Furthermore, the plane  $\Sigma_l$ , where the light source is located (figure 19), is positioned at distance  $d_2$ . We can describe an object as the binary function  $o: R^3 \rightarrow R$  in the following way:



$$o(\mathbf{r}_o) = \begin{cases} 0 & \text{if } \mathbf{r}_o \text{ is on the occluding regions of the object,} \\ 1, & \text{otherwise,} \end{cases} \quad (2)$$

where 1 means transmission and 0 opacity. We get the inverted object by defining the function  $1 - o(\mathbf{r}_o)$ . Similarly, we can define a binary function of the light source  $l: R^3 \rightarrow R$  with

$$l(\mathbf{r}_l) = \begin{cases} 1 & \text{if } \mathbf{r}_l \text{ is on the source,} \\ 0, & \text{otherwise,} \end{cases} \quad (3)$$

where 1 means luminous and 0 means not luminous. We will now consider a general representation of the projection of the object  $A_o$  that is produced by an arbitrary viewing point  $P$  on the screen. For this  $\mathbf{r}_i$  is an arbitrary but fixed vector in  $\Sigma_i$  pointing towards  $P$ . For a vector  $\mathbf{r}_o$  pointing towards  $A_o$  and the corresponding vector  $\mathbf{r}_l$  towards  $\Sigma_l$  we can formulate the relationship

$$\mathbf{r}_o - \mathbf{r}_l = \lambda \cdot (\mathbf{r}_i - \mathbf{r}_l), \quad (4)$$

which requires that  $\mathbf{r}_o - \mathbf{r}_l$  and  $\mathbf{r}_i - \mathbf{r}_l$  be linearly related with the vectors

$$\mathbf{r}_o = \begin{pmatrix} x_o \\ y_o \\ d_1 \end{pmatrix}, \mathbf{r}_l = \begin{pmatrix} x_l \\ y_l \\ d_1 + d_2 \end{pmatrix}, \mathbf{r}_i = \begin{pmatrix} x_i \\ y_i \\ 0 \end{pmatrix}. \quad (5)$$

Substituting the vectors in (5) into (4) gives the modification factor

$$\lambda = \frac{d_2}{d_1 + d_2}. \quad (6)$$

From (6) and (4) we obtain

$$\mathbf{r}_o = \frac{d_1 \cdot \mathbf{r}_l + d_2 \cdot \mathbf{r}_i}{d_1 + d_2}. \quad (7)$$

For a given point  $\mathbf{r}_i$  on the screen the function  $o(\mathbf{r}_o)$  in (2) is transformed by (7) into the projection  $o(\mathbf{r}_l, \mathbf{r}_i)$  on the plane of the light source. We can now define a new function  $\bar{l}(\mathbf{r}_l, \mathbf{r}_i) = l(\mathbf{r}_l)o(\mathbf{r}_l, \mathbf{r}_i)$  which is 1 when a point of the light source is visible from  $P$ , i.e. it is not obscured by the projected object. Therefore we get the value of the unobscured, i.e. the visible luminous area  $\bar{A}_l$  in  $\Sigma_l$

$$\bar{A}_l = \int_{\bar{A}_l} dA_l = \int_{\Sigma_l} \bar{l}(\mathbf{r}_l, \mathbf{r}_i) dA_l = \int_{\Sigma_l} l(\mathbf{r}_l)o(\mathbf{r}_l, \mathbf{r}_i) dA_l. \quad (8)$$

#### 4.3. Irradiance distribution in soft shadow images

The differential solid angle  $d\omega$  of the luminous area element  $dA_l$ , as seen from  $P$  at the angle  $\varepsilon_1$  and at the distance  $|\mathbf{r}_l - \mathbf{r}_i|$  is given by  $d\omega = dA_l \cos \varepsilon_1 \cdot |\mathbf{r}_l - \mathbf{r}_i|^{-2}$  (figure 20). For the radiant power  $d^2\Phi$  [W] transmitted from the surface element  $dA_l$  to  $dA_i$  we then obtain:

$$d^2\Phi = L dA_i \cos \varepsilon_2 d\omega = L \frac{dA_i \cos \varepsilon_2 \cdot dA_l \cos \varepsilon_1}{|\mathbf{r}_l - \mathbf{r}_i|^2}. \quad (9)$$

This relationship (9), also known as the *photometric fundamental law*, states that the radiant power transmitted from  $dA_l$  to  $dA_i$  is proportional to the apparent areas  $dA_l \cos \varepsilon_1$  and  $dA_i \cos \varepsilon_2$  and inversely proportional to the distance squared  $|\mathbf{r}_l - \mathbf{r}_i|^2$ , where  $L$  is the radiance from  $dA_l$  to  $dA_i$ . The radiated power towards the element  $dA_i$  from all elements  $dA_l$  of the

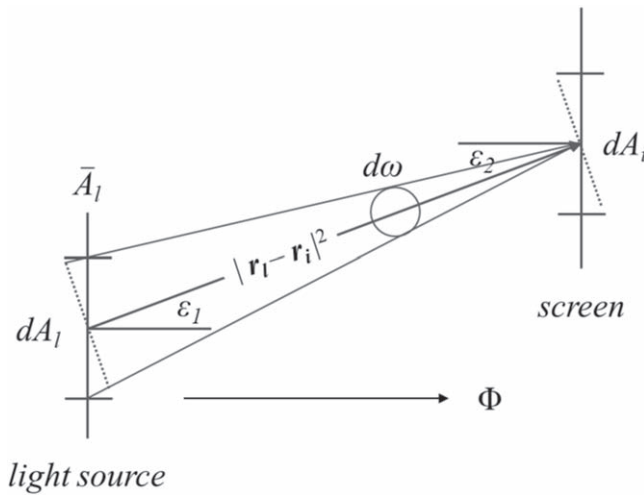


Figure 20. Radiant power on  $dA_i$ .

unobscured area light source  $\bar{A}_l$  visible from  $P$  gives the irradiance  $E(\mathbf{r}_i)$  [ $\text{W m}^{-2}$ ] at  $P$ :

$$E(\mathbf{r}_i) = d\Phi/dA_i = \int_{\bar{A}_l} L \frac{\cos \varepsilon_2 \cdot \cos \varepsilon_1}{|\mathbf{r}_l - \mathbf{r}_i|^2} dA_l. \tag{10}$$

The expression  $d\omega = \cos \varepsilon_1 \cdot |\mathbf{r}_l - \mathbf{r}_i|^{-2} \cdot dA_l$  takes into account the perspective shortening of the area light source and  $d\omega_p = d\omega \cdot \cos \varepsilon_2$  is the projected solid angle, which describes the orientation of the illuminated surface relative to the light source. From the geometric setting of the model, it follows from assumption (i) that  $\varepsilon_1 = \varepsilon_2$ . According to assumption (ii) we can replace the radiance  $L = M/\pi$ . Considering assumption (iii) of the paraxial approximation, we can set  $\cos \varepsilon_1 = \cos \varepsilon_2 \approx 1$  for small angles and  $|\mathbf{r}_l - \mathbf{r}_i| \approx d_1 + d_2$  for the distance. With these simplifications and with (8) the irradiance distribution (1) finally results in

$$E(\mathbf{r}_i) = \frac{M}{\pi(d_1 + d_2)^2} \int_{\bar{A}_l} dA_l = \frac{M}{\pi(d_1 + d_2)^2} \int_{\Sigma_l} l(\mathbf{r}_l) o(\mathbf{r}_l, \mathbf{r}_i) dA_l. \tag{11}$$

The expression  $\bar{A}_l/(d_1 + d_2)^2 = \bar{\Omega}_l$  corresponds to the solid angle of the visible area light source. Therefore,  $E(\mathbf{r}_i) \propto \bar{\Omega}_l$  is approximately valid under the given assumptions. If we use the substitution  $\mathbf{r}_l = -(d_2/d_1)\mathbf{r}'_l$ , (11) can be transformed with (7) into a convolution integral [8]. We obtain

$$E(\mathbf{r}_i) = \frac{M}{\pi(d_1 + d_2)^2} \left(\frac{d_2}{d_1}\right)^2 \int_{\Sigma_l} l\left(-\frac{d_2}{d_1}\mathbf{r}'_l\right) o\left(\frac{d_2(\mathbf{r}_i - \mathbf{r}'_l)}{d_1 + d_2}\right) dA'_l \tag{12}$$

$$= \frac{Md_2^2}{\pi d_1^2(d_1 + d_2)^2} l\left(-\frac{d_2}{d_1}\mathbf{r}_i\right) * o\left(\frac{d_2}{d_1 + d_2}\mathbf{r}_i\right). \tag{13}$$

We obtain from (11) the irradiance distribution  $E_1^C$  for inverted objects or  $E_2^C$  for inverted light sources (bright shadow situation) by replacing  $o(\mathbf{r}_l, \mathbf{r}_i)$  by  $1 - o(\mathbf{r}_l, \mathbf{r}_i)$  in the first case and  $l(\mathbf{r}_l)$  by  $1 - l(\mathbf{r}_l)$  in the second case. To confirm the relation for complementarity (1) in each case, we add either  $E_1^C$  or  $E_2^C$  to  $E(\mathbf{r}_i)$  from (11). In the first case, we get

$$E(\mathbf{r}_i) + E_1^C(\mathbf{r}_i) = \frac{M}{\pi(d_1 + d_2)^2} \int_{\Sigma_i} l(\mathbf{r}_l) dA_l = \frac{MA_l}{\pi(d_1 + d_2)^2} = E_0, \quad (14)$$

which is a constant for fixed distance  $d_1 + d_2$ . Inverse objects therefore, lead to complementary shadow images. For the second case, we obtain

$$E(\mathbf{r}_i) + E_2^C(\mathbf{r}_i) = \frac{M}{\pi(d_1 + d_2)^2} \int_{\Sigma_i} o(\mathbf{r}_l, \mathbf{r}_i) dA_l. \quad (15)$$

Due to the definition of  $o(\mathbf{r}_l, \mathbf{r}_i)$  the integral in (15) diverges. In practice, the nonluminous geometry of the inverted light source is embedded in a luminous area of finite size. Therefore the integral is constant for every location  $P$ . It follows, that the bright shadow is also a complementary shadow phenomenon.

#### 4.4. Test of the model

An analytical closed-form solution is not possible even for simple geometries, so all calculations are numerical, performed with *Mathematica*. For comparability of the model and experimental data, we used the relative irradiance  $E/E_0 = \bar{A}_l/A_l$ . The range of values of (8) was mapped to a linear grayscale between white and black (8-bit), where we set the endpoints to black for 0 ( $\bar{A}_l = 0$ , the light source is not visible) and to white for 1 ( $\bar{A}_l = 1$ , the light source is completely visible).

We will apply the model to the L-shaped light source and the square object from figure 13 with the ratio of their edge lengths of 4: 1. For (3) of the source we let

$$l(\mathbf{r}_l) = \begin{cases} 1 & \text{if } (-4.5 \leq x_l, y_l \leq 4.5) \vee (-4.5 \leq x_l \leq 0 \wedge 0 \leq y_l \leq 4.5) \\ 0, & \text{otherwise} \end{cases} \quad (16)$$

and with (2) for the obstacle we let

$$o(\mathbf{r}_o) = \begin{cases} 0 & \text{if } (-2.25 \leq x_o, y_o \leq 2.25) \\ 1, & \text{otherwise.} \end{cases} \quad (17)$$

We chose the distance to be  $d_1 + d_2 = 240$ . Figure 21 shows for different stages  $d_1/d_2$  the computed transformation of the shadow images for an obstacle (below) and the inverse aperture (above). The values  $d_1/d_2$  were chosen so that the model reproduces the transformation characteristics of the shadow images from figure 9.

For experimental testing of the predicted irradiance distribution (11) we used a light source which allows to realize extended fields of homogeneous radiosity [42]. It consists of a hemisphere ( $\emptyset = 30$  cm), the inside of which is coated with a high-matte white and is illuminated with  $4 \times 500$ W halogen lamps. In front of the opening can be placed apertures cut from sheet steel with different geometries. The distances were set to  $d_1/d_2 = 1$ . The photos of the shadow images were taken with a photo camera (Nikon D60, Sigma DC 1008072). A camera usually has a nonlinear grayscale value output. To avoid this problem, we used RAW files (NEF) for the analysis, where the camera writes the data to the storage medium after digitization largely without processing. For lossless image editing, the RAW files were converted compression-free into an 8-bit grayscale TIFF-image. To ensure the linear grayscale, all further image editing was performed without any gamma-correction ( $\gamma = 1$ ). Using tone correction, we mapped the photo to a scale from black to white. Furthermore, the image analysis shows noise superimposed on the irradiance distribution due to the graininess of the screen. We averaged out the fluctuations by local blurring. The photographs edited in this way were analyzed with the image processing program *Image Analyzer*.

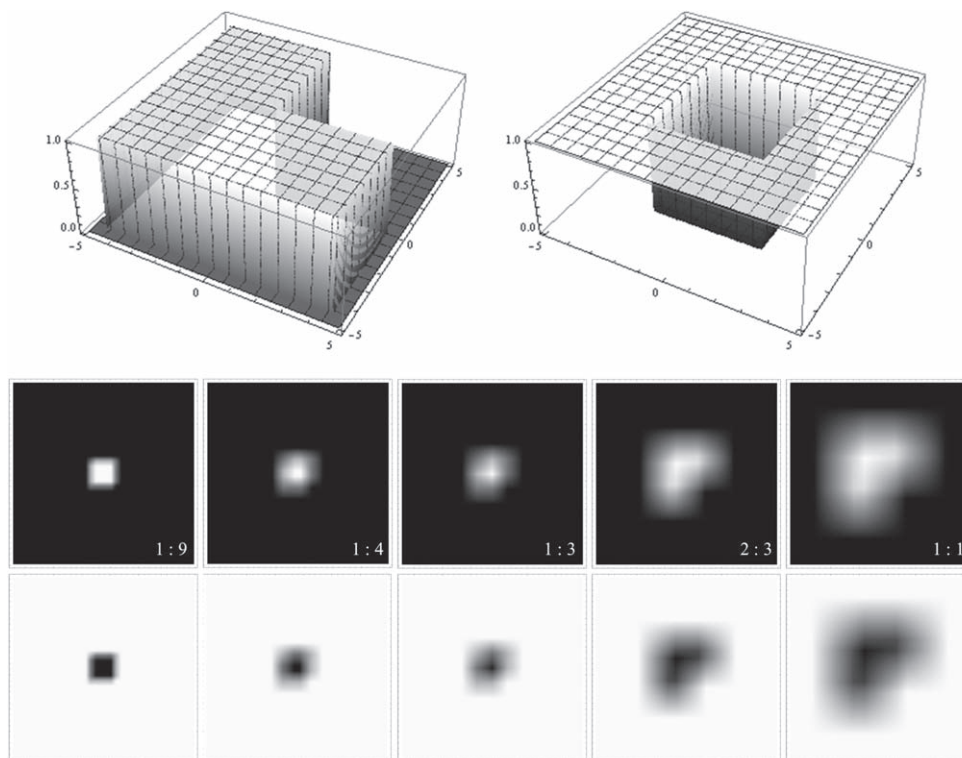


**Figure 21.** Above: The function of the light source (16) and the obstacle (17). Below: computed transformation of soft shadow images produced by aperture (above) and obstacle (below) for a L-shaped light source and different stages  $d_1/d_2$ . Compare the respective setup in figure 13 and the photographs in figure 9.

Not only do figures 22 and figure 23 show remarkable agreement between the photographed and computed shadow images in the visual inspection, comparing  $E/E_0$  for the selected profile lines allows a quantitative reproduction of the characteristic irradiance distributions by the model.

## 5. Summary

Our primary goal in this paper was to provide the reader with an overview of multiple shadow phenomena that can be motivationally accessed with the embedded perspective. For practical teaching, we can only give some hints at this point. The material for soft shadow images presented in this paper provides several starting points for teaching optics at both the high school level and the undergraduate level.

The idea of the embedded view makes difficult irradiances on the projection screen understandable even to students at the undergraduate level. ‘Bright is where bright can be seen from’ sounds almost trivial, but operated systematically, leads to basic imaging principles in shadow imaging. Even without the theoretical model, students can understand the transformation behavior or the irradiance distribution of shadow images [43]. In addition, the connection to their own visual experience can motivate and increase the feeling of self-efficacy. The approach of the embedded perspective can also be applied to other optical

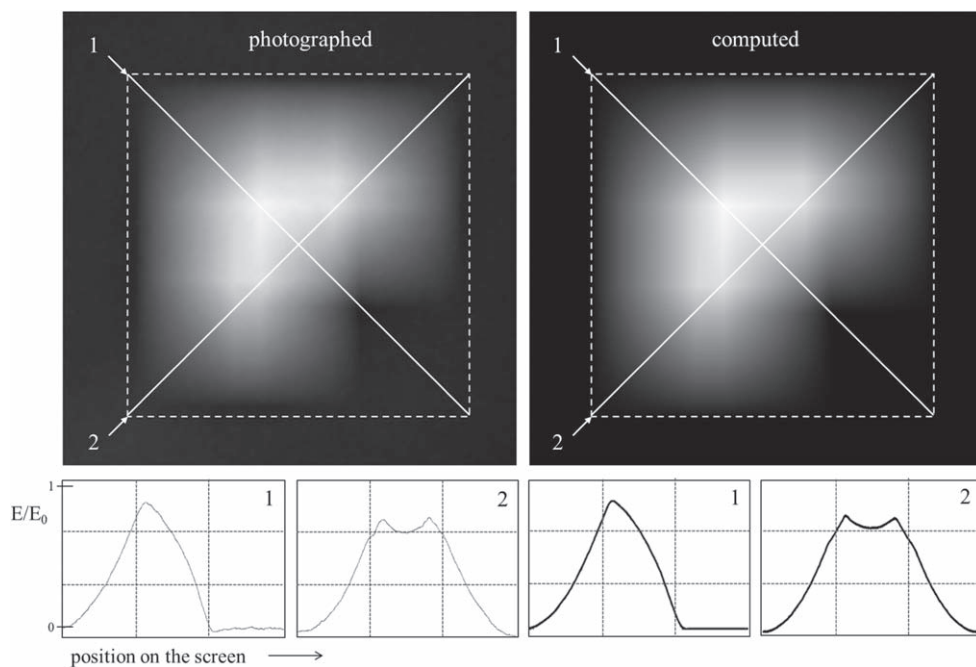


**Figure 22.** Left: The photo of the shadow image was taken with an exposure time of 0.125 s, an aperture of  $f/10$  and a sensitivity of ISO400. Right: The corresponding computed shadow image. Below: the measured curves of  $E/E_0$  together with the theoretical curves as predicted by the model for the two lines 1 and 2.

contexts such as the mirror, the lens or diffraction and can therefore also be used in optics lessons [26, 44–48].

Shadows have long been part of the canon of optics education, usually focusing on special cases. Either one considers hard shadows caused by point light sources or pinhole camera images caused by expansionless apertures. As was shown, the shadow image generally contains geometric information of both the object and the light source, i.e. both have an imaging effect at the same time. As we have also seen, soft shadow images can be generalized by the principles of complementarity and inversion. In the classroom, the example of shadow images can illustrate how the same imaging laws are at work in the variety of shadow phenomena and provides an example of the idea of unification—an important principle in physics. From a more technical perspective, students may be interested in how to reconstruct the geometries of the light source and object from a given shadow image [49, 50].

As shown in (12), the integral in (11) can be written as a convolution product. This is an important result because it means that the irradiance distribution is finally the consequence of a convolution operation between the geometries of the object and light source. Thus, a fundamental concept of convolution, whose first important application is usually the lens, can already be introduced in shadow images. The same applies to the ideas of complementarity and inverse objects, which proved fruitful here, and which reappear in the context of complementary colors and spectra [33]. Thus, the shadow image not only offers access to some high-level optical ideas, but it is also a nice example of what Berry called *the arcane in the mundane*, i.e. ‘to bring out connections between what can be seen with the unaided, or almost

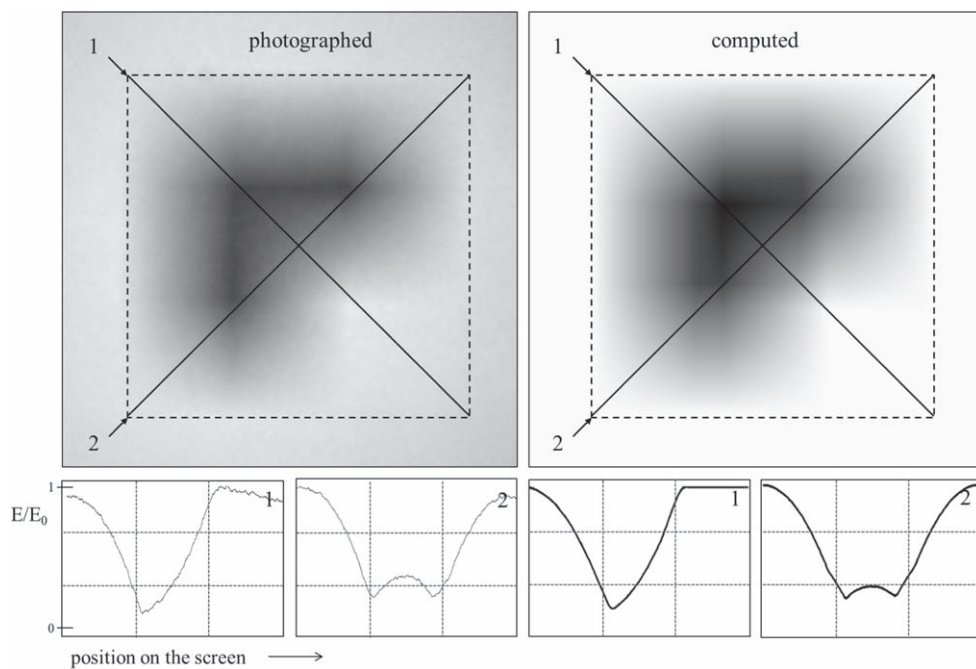


**Figure 23.** Left: The photo of the complementary shadow image was taken with an exposure time of 1.3 s, an aperture of  $f/14$  and a sensitivity of ISO400. Right: the computed shadow image. Below: the measured curves of  $E/E_0$  together with the theoretical curves.

unaided, eye and general explanatory concepts in optics and more widely in physics and mathematics' [51].

Shadows are ubiquitous and speak to our sense of beauty. They offer several starting points for teaching optics, provide insights into modern imaging techniques and can still lead to exciting discoveries like the bright shadow.

### Acknowledgments


The authors thank all anonymous referees for improving the clarity and presentation of this document. In particular, we would like to thank the second reviewer for the idea to illustrate the embedded perspective by the setup shown in figure 13 and for a valuable discussion.

### Data availability statement

All data that support the findings of this study are included within the article (and any supplementary files).

### ORCID iDs

Johannes Grebe-Ellis  <https://orcid.org/0000-0003-0400-0780>

Thomas Quick  <https://orcid.org/0000-0002-9201-6231>

## References

- [1] Feher E and Rice K 1988 *Sci. Educ.* **72** 637–49
- [2] Dedes C and Ravanis K 2009 *Sci. Educ.* **18** 1135–51
- [3] Cohen A L 1982 *Opt. Acta* **29** 63–7
- [4] Torralba A and Freeman W 2014 *Int. J. Comput. Vis.* **110** 92–112
- [5] Annen T, Mertens T, Bekaert P, Seidel H-P and Kautz J 2007 *Rendering Techniques* The Eurographics Association
- [6] Eisemann E, Assarsson U, Schwarz M and Wimmer M 2010 Eurographics 2010 Tutorial Notes ([www.iosrjournals.org](http://www.iosrjournals.org)) (<http://research.michael-schwarz.com/publ/files/shadowcourse-eg10.pdf>)
- [7] Hasenfratz J M, Lapierre M, Holzschuch N and Sillion F X 2003 *Comput. Graph. Forum* **22** 753–74
- [8] Soler C and Sillion F 1998 Fast calculation of soft shadow textures using convolution *SIGGRAPH '98 (Proceedings of the 25th Annual Conference on Computer Graphics and Interactive Techniques)* pp 321–32
- [9] Grebe-Ellis J 2010 *PhyDid A* **9** 34–44
- [10] Maier G 2011 *An Optics of Visual Experience* (New York: Adonis Press)
- [11] Grebe-Ellis J 2007 Lesen im Buch der Natur *Didaktik der Physik. (Beiträge zur Frühjahrstagung der DPG.) (Regensburg)* ed V Nordmeier and A Oberländer (Berlin: Lehmanns Media) pp 1–12 ([https://researchgate.net/publication/281652133\\_Lesen\\_im\\_Buch\\_der\\_Natur\\_Zur\\_Entwicklung\\_einer\\_phanomeno-logischen\\_Lesekompetenz](https://researchgate.net/publication/281652133_Lesen_im_Buch_der_Natur_Zur_Entwicklung_einer_phanomeno-logischen_Lesekompetenz))
- [12] Erb R and Grebe-Ellis J 2011 *Alles, wozu der Mensch sich ernstlich einlässt, ist ein Unendliches* (Berlin: Logos Verlag) p 55
- [13] Lynch D K and Livingston W 2001 *Color and Light in Nature* (Cambridge: Cambridge University Press) p 1
- [14] Naylor J 2002 *Out of the Blue* (Cambridge: Cambridge University Press) p 29
- [15] Baez A V 1957 *Am. J. Phys.* **25** 636
- [16] Ambrosini D and Spagnolo G S 1997 *Am. J. Phys.* **65** 256–7
- [17] Flynt H and Ruiz M J 2015 *Phys. Educ.* **50** 19
- [18] Greenslade T B Jr. 1994 *Phys. Teach.* **32** 347
- [19] Hewitt P 2000 *Phys. Teach.* **38** 272
- [20] Mallmann A J 2013 *Phys. Teach.* **51** 10–1
- [21] Schlichting H J 1995 *MNU* **48** 199–207
- [22] Möllmann K P and Vollmer M 2006 *Eur. J. Phys.* **27** 1299–314
- [23] Grebe-Ellis J 2006 *Chim. Didact.* **32** 137–86 ([https://physikdidaktik.uni-wuppertal.de/fileadmin/physik/didaktik/Forschung/Publikationen/Grebe-Ellis/Grebe-Ellis\\_Phaeno\\_Optik\\_1.pdf](https://physikdidaktik.uni-wuppertal.de/fileadmin/physik/didaktik/Forschung/Publikationen/Grebe-Ellis/Grebe-Ellis_Phaeno_Optik_1.pdf))
- [24] Østergaard E, Dahlin B and Hugo A 2008 *Stud. Sci. Educ.* **44** 93–121
- [25] Park W and Song J 2018 *Sci. Educ.* **27** 39–61
- [26] Grusche S 2019 *J. Phys. Conf. Ser.* **1287** 012066
- [27] Spiecker H and Bitzenbauer P 2022 *Phys. Educ.* **57** 045012
- [28] Sebald J, Fliegau K, Veith J, Spiecker H and Bitzenbauer P 2022 *Physics* **4** 1117–34
- [29] Fliegau K, Sebald J, Veith J, Spiecker H and Bitzenbauer P 2022 *Optics* **3** 409–29
- [30] Lipson A, Lipson S and Lipson H 2010 *Physical Optics* (Cambridge: Cambridge University Press)
- [31] Hecht E 2016 *Optics* (Essex: Pearson Education)
- [32] Meyn J P 2008 *Eur. J. Phys.* **29** 1017–31
- [33] Babič V and Čepič M 2009 *Eur. J. Phys.* **30** 793–806
- [34] Rang M, Passon O and Grebe-Ellis J 2017 *Phys. J.* **16** 43–9
- [35] Minnaert M 2003 *The Nature of Light and Colour in the Open Air* (New York: Dover Publications)
- [36] Rang M 2015 *Phänomenologie Komplementärer Spektren* (Berlin: Logos Verlag)
- [37] Quick T, Müller M and Grebe-Ellis J 2009 Mathematische Beschreibung von Schattenbildern *Didaktik der Physik. (Beiträge zur Frühjahrstagung der DPG.) (Bochum)* ed V Nordmeier and A Oberländer (Berlin: Lehmanns Media) pp 1–8 ([https://researchgate.net/publication/281652350\\_Mathematische\\_Beschreibung\\_von\\_Schattenbildern\\_im\\_Kontext\\_der\\_phanomenologischen\\_Optik](https://researchgate.net/publication/281652350_Mathematische_Beschreibung_von_Schattenbildern_im_Kontext_der_phanomenologischen_Optik))
- [38] Lynch D K 2015 *Appl. Opt.* **54** 154–64
- [39] English R E Jr. and George N 1988 *Appl. Opt.* **27** 1581–87

- [40] Enright J T 1994 *Appl. Opt.* **33** 4723–26
- [41] Huang A E, Hon A J and Altschuler E L 2008 *Perception* **37** 1458–60
- [42] Holtsmark T 1976 *Halbschatten und Bild. Mathematisch-Physikalische Korrespondenz* **100** 3–10
- [43] Schön L H 1994 *Physik in der Schule* **32** 2–5
- [44] Sommer W and Grebe-Ellis J 2010 *Proc. Int. Conf. Contemporary Science Education Research: International Perspectives* vol 3 (Ankara: Pegem Akademi) pp 77–83
- [45] Sommer W 2013 *Eur. J. Phys.* **34** 259–71
- [46] Grusche S 2016 *Phys. Edu.* **51** 015006
- [47] Grusche S 2017 *Phys. Edu.* **52** 044002
- [48] Grusche S 2018 *Ein bildbasierter Zugang zur Linsenabbildung und Spektroskopie.* (<https://hsbwgt.bsz-bw.de/frontdoor/index/index/start/0/rows/10/sortfield/score/sortorder/desc/searchtype/simple/query/grusche/docId/266>) Pädagogische Hochschule Weingarten
- [49] Bouman K L *et al* 2017 *EEE Int. Conf. on Computer Vision (ICCV)* pp 2270–78
- [50] Saunders C, Murray-Bruce J and Goyal V K 2019 *Nature* **565** 472–75
- [51] Berry M V 2015 *Contemp. Phys.* **56** 2–16